Chemistry & Biology, *18*

Supplemental Information

Rational Design of Photoconvertible and Biphotochromic Fluorescent Proteins for Advanced Microscopy Applications

Virgile Adam, Benjamien Moeyaert, Charlotte C. David, Hideaki Mizuno, Mickaël Lelimousin, Peter Dedecker, Ryoko Ando, Atsushi Miyawaki, Jan Michiels, Yves Engelborghs, and Johan Hofkens

Supplemental Information Inventory

Figure S1, related to Figure 1

Table S1, related to Figure 1

Figure S2, related to Figure 4

Figure S3, related to Figure 4

Figure S4, related to Figure 2

Figure S5, related to Figure 2

Table S2, related to Figure 3

Table S3, related to Figure 3

Figure S6, related to Figure 5

Figure S7, related to Figure 5

Supplemental Experimental Procedures

Figure S1

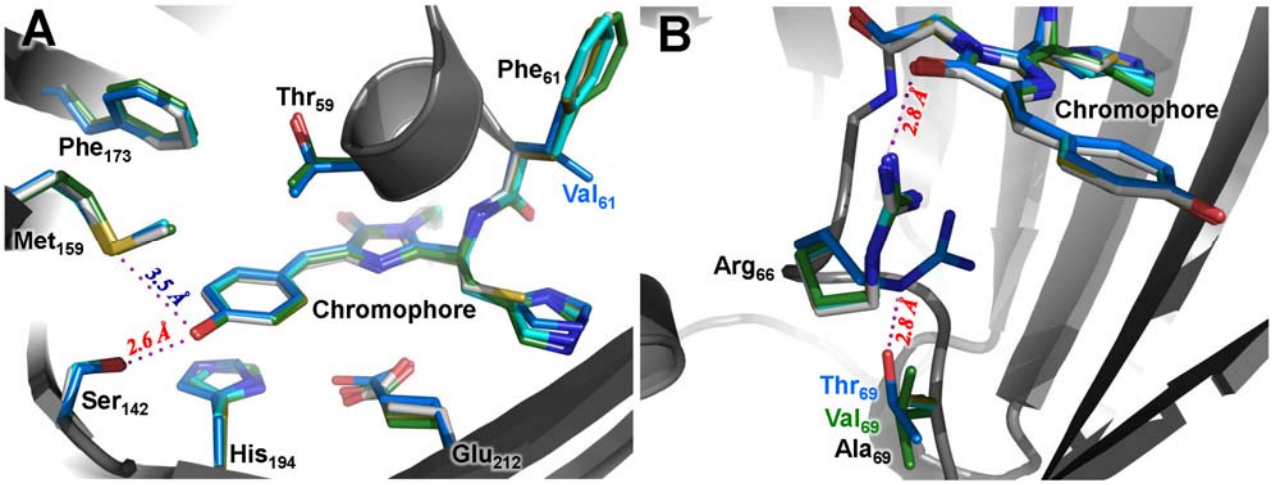
A
Phe173
Thr59
Phe61
Val61
Met159
3.5 Å
2.6 Å
Chromophore
Ser142
His194
Glu212
B
2.8 Å
Chromophore
Arg66
2.8 Å
Thr69
Val69
Ala69

Figure S2

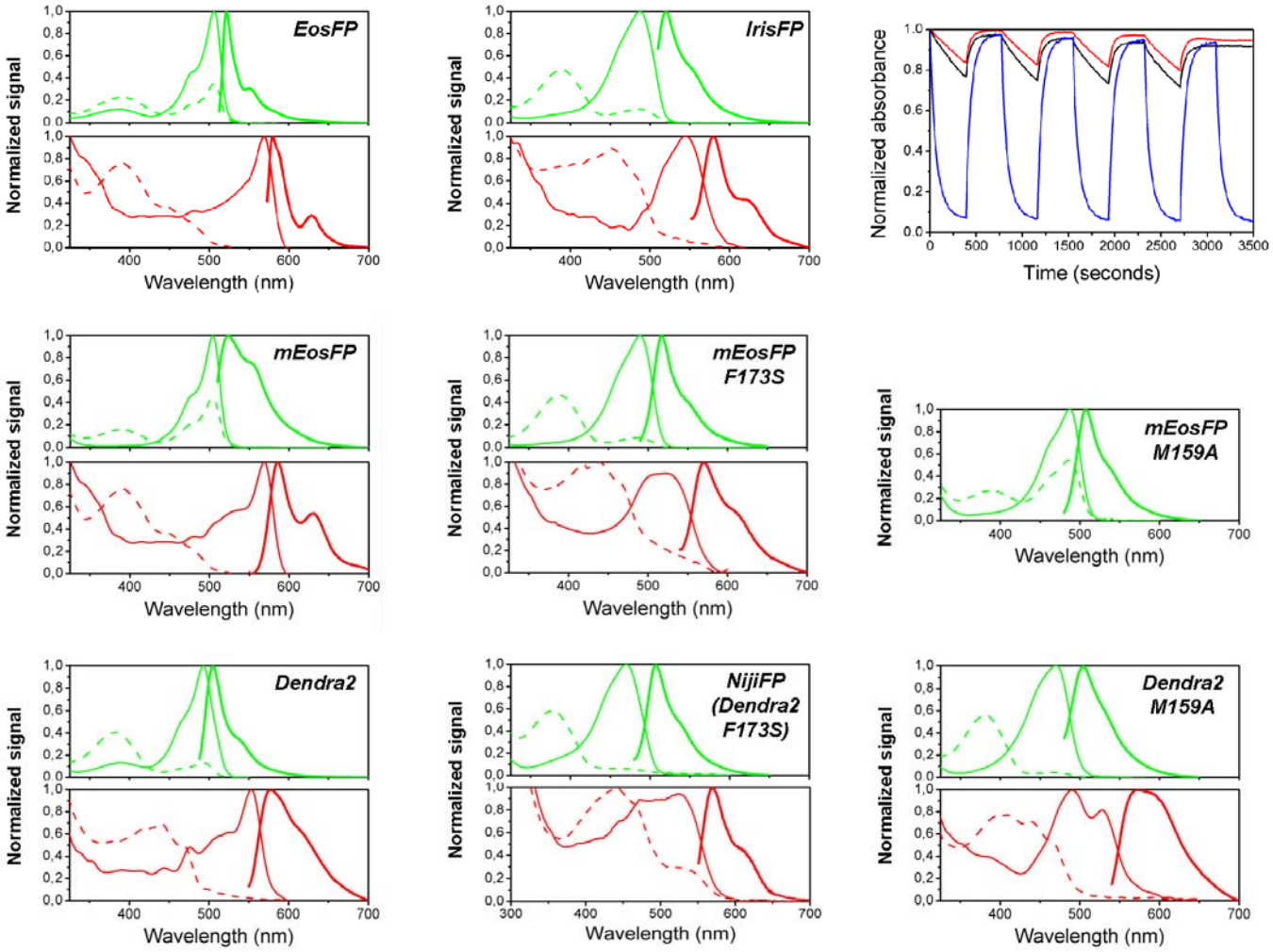
EosFP
IrisFP
Normalized absorbance
Time (seconds)
mEosFP
mEosFP F173S
mEosFP M159A
Dendra2
NijiFP (Dendra2 F173S)
Dendra2 M159A
Normalized signal
Wavelength (nm)

Figure S3

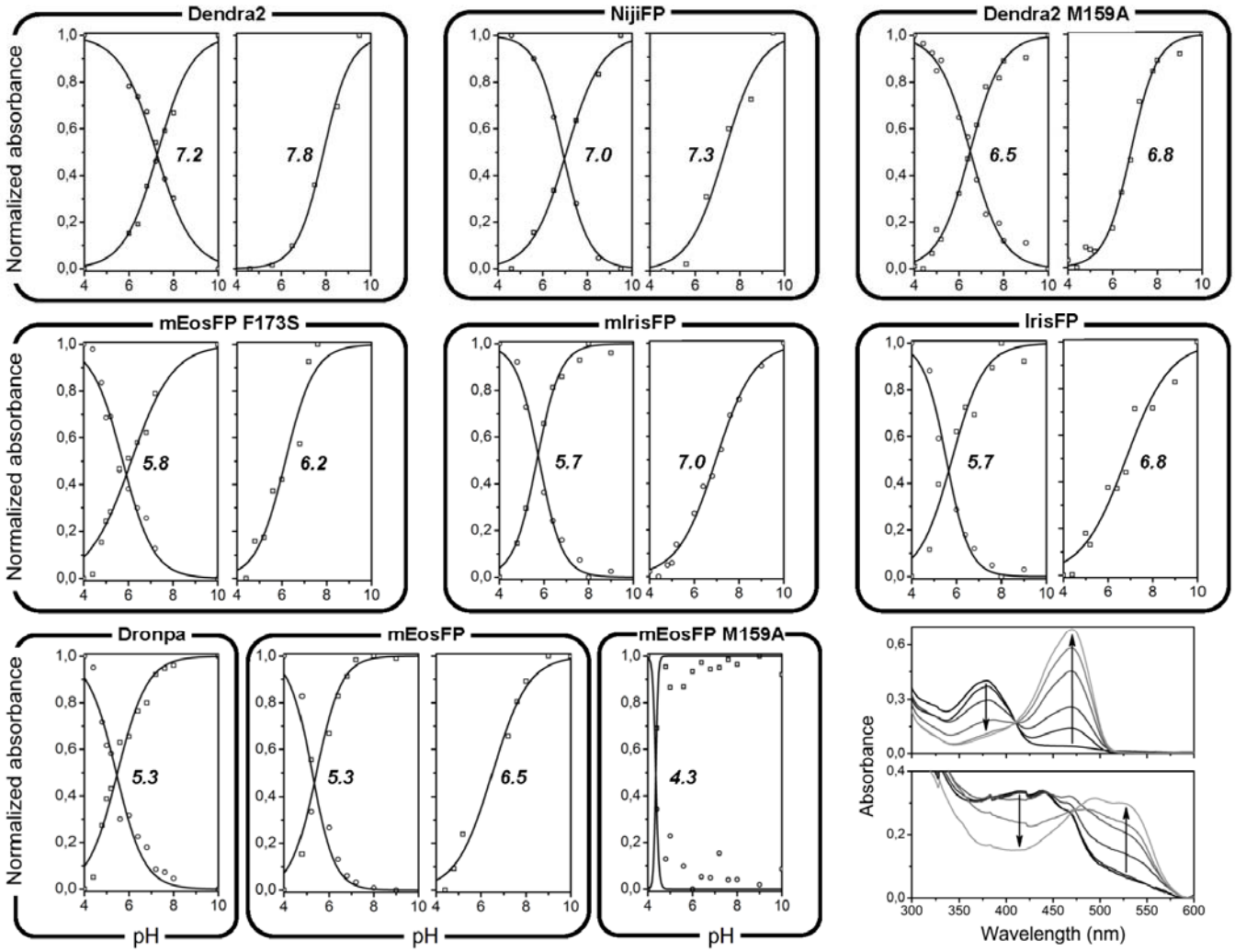
Dendra2
7.2
7.8
NijiFP
7.0
7.3
Dendra2 M159A
6.5
6.8
mEosFP F173S
5.8
6.2
mIrisFP
5.7
7.0
IrisFP
5.7
6.8
Dronpa
5.3
mEosFP
5.3
6.5
mEosFP M159A
4.3
Normalized absorbance
pH
Absorbance
Wavelength (nm)

Figure S4

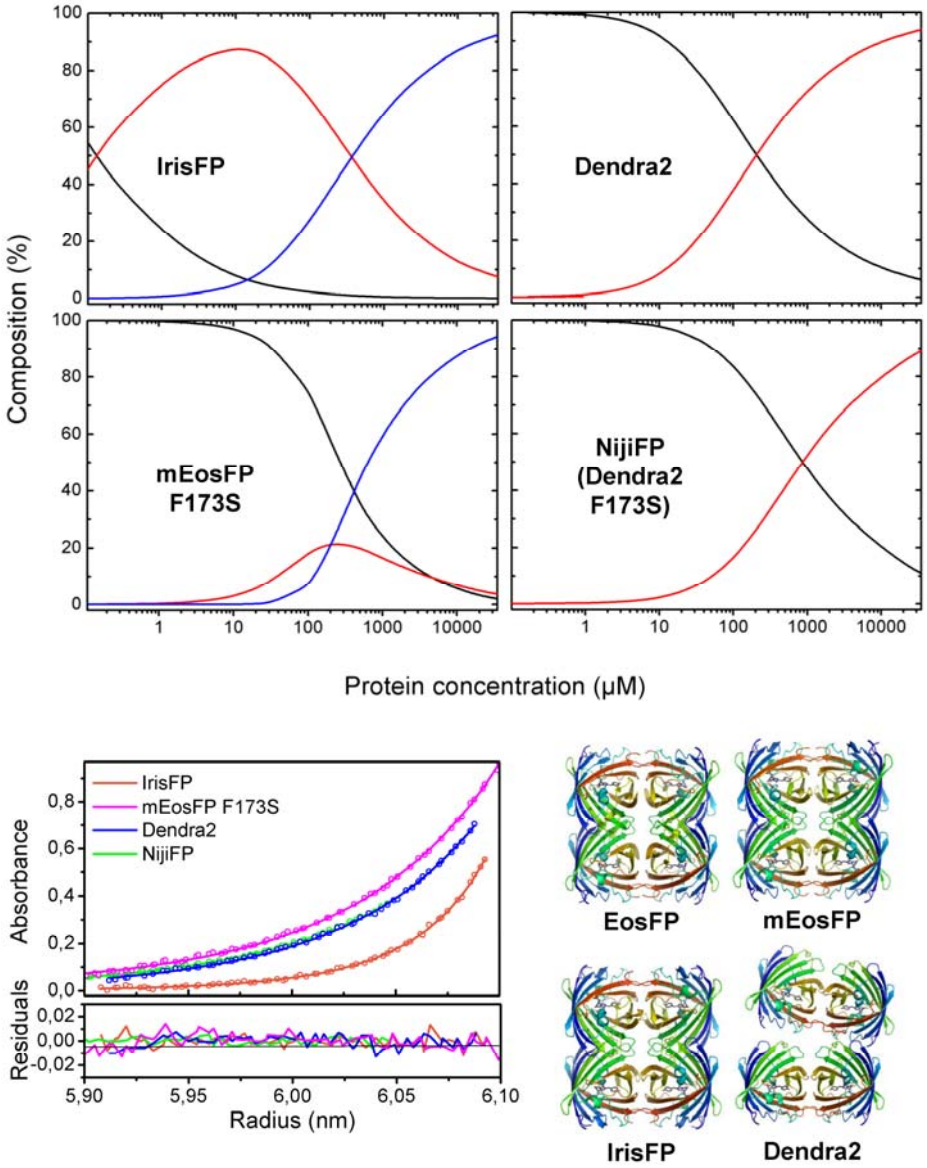
IrisFP
Dendra2
mEosFP
F173S
NijiFP
(Dendra2
F173S)
Composition (%)
Protein concentration (μM)
IrisFP
mEosFP F173S
Dendra2
NijiFP
Absorbance
Residuals
Radius (nm)
EosFP
mEosFP
IrisFP
Dendra2

Figure S5

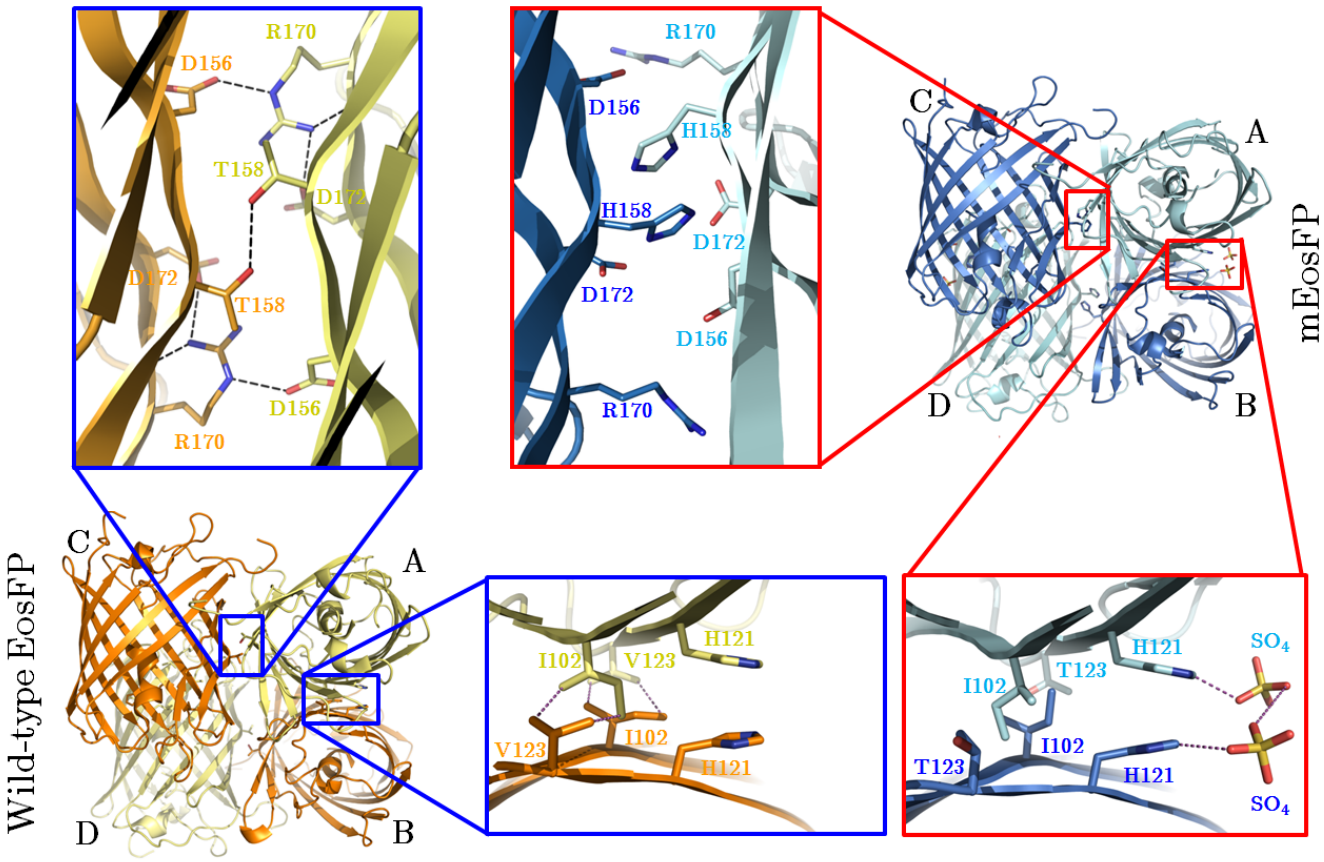
R170
D156
T158
D172
D172
T158
D156
R170
R170
D156
H158
H158
D172
D172
D156
R170
C
A
D
B
mEosFP
Wild-type EosFP
C
A
D
B
H121
I102
V123
V123
I102
H121
H121
SO4
T123
I102
I102
T123
H121
SO4

Figure S6

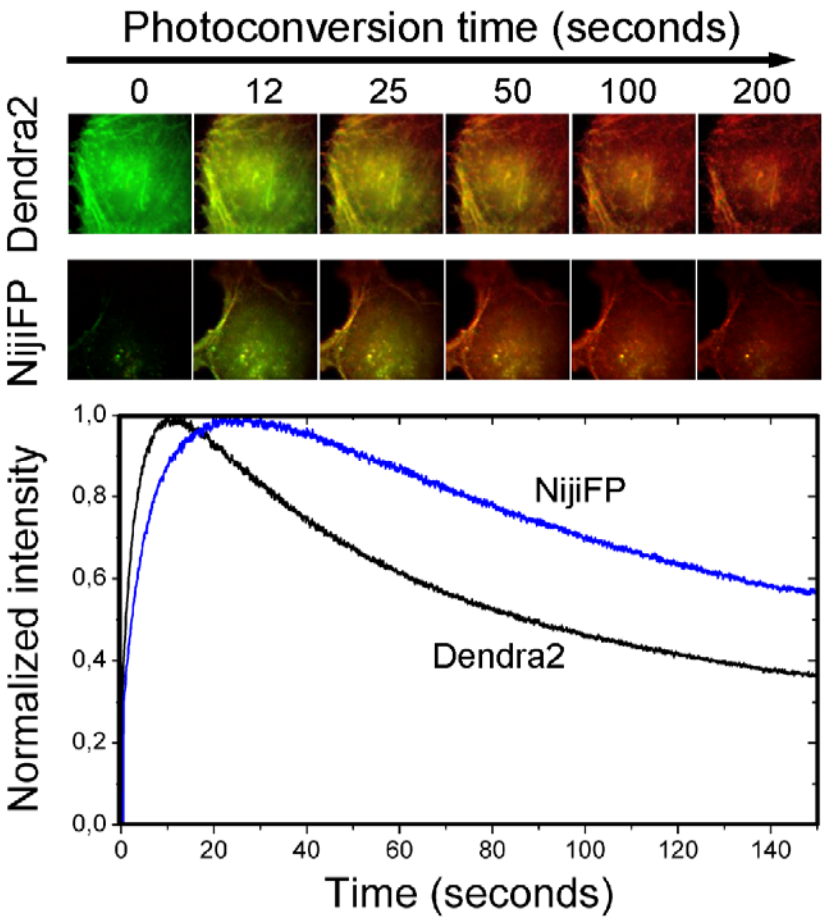
Photoconversion time (seconds)
0
12
25
50
100
200
Dendra2
NijiFP
Normalized intensity
1,0
0,8
0,6
0,4
0,2
0,0
0
20
40
60
80
100
120
140
Time (seconds)
NijiFP
Dendra2

Figure S7

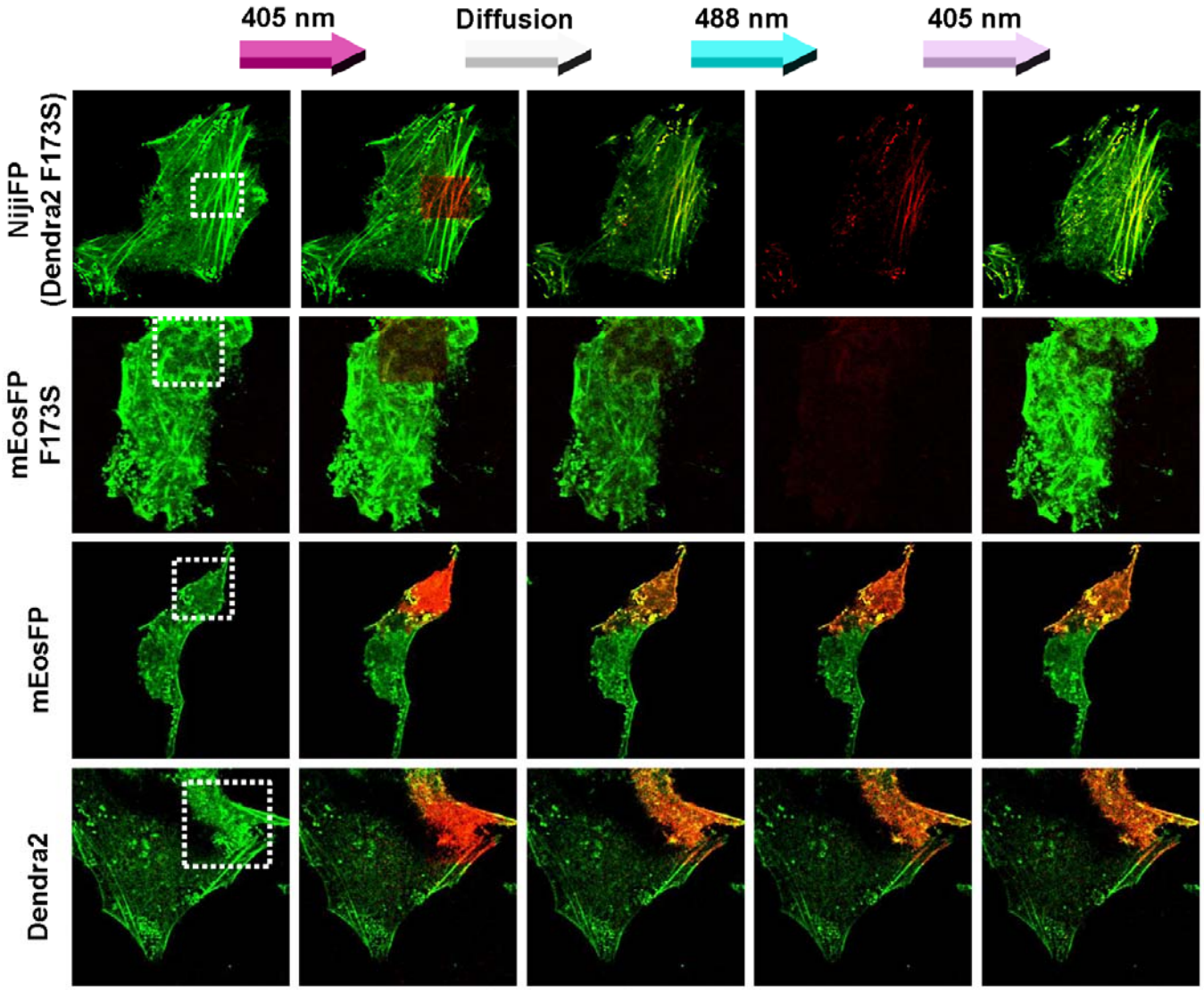
405 nm
Diffusion
488 nm
405 nm
NijiFP (Dendra2 F173S)
mEosFP F173S
mEosFP
Dendra2

FIGURE LEGENDS

Figure S1, related to Figure 1. Structural overlay of several photoactivatable fluorescent proteins.

(A) The chromophores of several commonly used RSFPs and PCFPs and their microenvironment are overlaid: mEosFP (cyan, PDB: 3P8U), KikGR (green, PDB: 2DDD), Dendra2 (blue, PDB: 2VZX), Dronpa (white, PDB: 2Z1O) and Kaede (golden, PDB: 2GW3), showing their very high structural identity. (B) The electrostatic interaction between Arg66 and the chromophore is disrupted in the case of Dendra2 (due to the direct interaction between Thr69 and Arg66), increasing the fraction of neutral form and promoting photoconversion in this fluorescent protein. H-bonds and Van der Waals interactions are represented in red and blue distance labels, respectively.

Figure S2, related to Figure 4. Absorption and emission spectra of green and red states of EosFP, Dendra2 and their mutants.

Absorption spectra are represented in dotted (pH 4) and solid (pH 9) lines. Fluorescence emission spectra are shown as a thicker solid line. The top-right panel represents the photoswitching timecourse of mEosFP (red), Dendra2 (black) and NijiFP (Dendra2 F173S, blue) solutions. The samples were repeatedly irradiated with 488-nm and 405-nm light while the peak absorption was recorded every 7.5 seconds.

Figure S3, related to Figure 4. Chromophoric protonation of green and red states of the proteins as a function of pH (ordered by decreasing pKa).

To calculate pKa values of each protein's chromophore, the maximum absorption peaks of anionic (squares) and neutral (circles) states were measured between pH 4 and 10 and the titration was fitted to a Henderson-Hasselbalch relation (sigmoid curves). While the evolution of both peaks was fitted for the green states (left-hand part in each panel), only the anionic peak was followed in the red states (right-

hand part of each panel) to avoid errors in incompletely photoconverted proteins since the neutral state of the red species and the anionic state of the green species generally overlay. Dronpa and mEosFP M159A are not photoconvertible to the red and thus only the evolutions of their anionic and neutral states in their green states were followed. The bottom-right spectra depict typical absorption measurements with the example of NijiFP (Dendra2 F173S) in green (top) and red (bottom) states. The arrows indicate the pH increase.

Figure S4, related to Figure 2. Concentration-dependent oligomerization of Dendra2, mEosFP and their mutants. Comparison between the Dendra2 and EosFP-derived crystal packings.

The first four panels show the composition of monomer (black), dimer (red), and tetramer (blue) in Dendra2, NijiFP (Dendra2 F173S), IrisFP and mEosFP F173S estimated from the association constants. The two bottom panels represent the equilibrium radial absorbance of the four proteins and the content of the asymmetric unit of the crystallographic structures of EosFP, mEosFP, IrisFP and Dendra2.

Figure S5, related to Figure 2. Quaternary organization in crystal structures of EosFP and mEosFP.

At the interface A/B of EosFP wild-type (PDB: 1ZUX), the interactions between Ile102 and Val123 cease when Val123 is mutated to a threonine in mEosFP (PDB: 3P8U). At the interface A/C, while a complex network of contacts between Asp156, Thr158, Arg170 and Asp172 forms a strong interaction between respective chains in EosFP, the mutation of Thr158 into a histidine disrupts most of this network in mEosFP. However, at both interfaces, a pair of histidines of respective chains (His158 for the interface A/C and His121 at the interface A/B), form π-stackings that are probably responsible for the tetrameric organization of mEosFP in its crystal structure (reinforced by sulfate ions at the interface A/B) and the tendency of this protein to form oligomers at increasing concentrations.

Figure S6, related to Figure 5. Photoconversion and photostability of Dendra2 and NijiFP (Dendra2 F173S) in cells.

HeLa cells expressing Dendra2- and NijiFP-fused actin were photoconverted with continuous 405-nm light while green and red fluorescence signals were measured with weak pulses of 488 and 561-nm light, respectively. (A) Wide-field images with merged green and red channels allow the observation of the cell along the photoconversion process. As seen on the first panel for NijiFP, the green fluorescence signal was switched-off during the time needed to localize the cell with 488-nm light. Prior the observation of any photoconversion, this green emission is readily recovered as soon as the 405-nm light is used. The actual size of each panel is 41 × 41 μm. (B) To provide an estimate for the photoconversion to and the photostability of the red form of Dendra2 (black line) and NijiFP (blue line) the total intensity of the red channel was integrated and plotted in time. This clearly shows the green-to-red photoconversion (increase) preceding the slower photobleaching (decrease).

Figure S7, related to Figure 5. NijiFP-, mEosFP F173S-, Dendra2- and mEosFP-labeled actin as imaged using a confocal microscope.

First, proteins in a specific region of interest were photoconverted from the green to the red state using 405-nm light. The cells were kept at room temperature to allow the intracellular dynamics of actin. Subsequently, the green fluorescence was switched off using 488-nm light and recovered using 405-nm light. Intensity scales for green and red emission are identical for all pictures. Scale bar: 20 μm.

TABLES

Table S1, related to Figure 1. Optical properties of photoswitchable and photoconvertible fluorescent proteins discussed.

Fluorescent protein	Parent	Mutations	Reversible photo-switching	Green-to-red photo-conversion	Reference
Dronpa			+	–	(Ando et al., 2004)
Dronpa-2	Dronpa	M159T	++	–	(Ando et al., 2007)
Dronpa-3	Dronpa	V157I M159A	+++	–	(Ando et al., 2007)
rsFastLime	Dronpa	V157G	+++	–	(Stiel et al., 2007)
bsDronpa	Dronpa	V157G M159C F173C	+++	–	(Andresen et al., 2008)
Padron*	Dronpa	V157G M159Y	+++	–	(Andresen et al., 2008)
EosFP			–	+	(Wiedenmann et al., 2004)
mEosFP	EosFP	V123T T158H (A69V)	–	+	(Wiedenmann et al., 2004)
IrisFP	EosFP	F173S	+++	+	(Adam et al., 2008)
mIrisFP	mEosFP	A69V F173S K145I Y189A	+++	+	(Fuchs et al., 2010)
mEosFP-M159A	mEosFP	M159A	++	–	This work
mEosFP-F173S	mEosFP	A69V F173S	++	+	This work
Dendra2			–	++	(Gurskaya et al., 2006)
Dendra2-M159A	Dendra2	M159A	++	+	This work
NijiFP	Dendra2	F173S	++	++	This work

* Positive switching

Table S2, related to Figure 3. Data collection, refinement and structure quality statistics of mEosFP. (PDB ID: 3P8U).

Data collection statistics		Refinement statistics	
Beamline	ESRF / ID14-3	R_{cryst}/R_{free}[c]	0.221 / 0.284
Wavelength, Å	0.931	No. of atoms (protein)	7769 (7288)
Space group	$P2_12_12_1$	No. of water	386
Cell dimensions		Rmsd bond lengths, Å	0.015
a, *b*, *c*, Å	86.45, 96.82, 140.43	Rmsd bond angles, °	1.606
α, β, γ, °	90, 90, 90	Average B factor, Å^2	
Resolution, Å	48.4-2.25 (2.5-2.25)[a]	All atoms	33.2
R_{sym}, %[b]	7.9 (51.3)	Chromophore	27.9
Mean $I/\sigma(I)$	15.7 (3.1)	Ramachandran plot	
Completeness, %	92.8 (99.5)	Most favored region, %	98.6
No. of total reflections	274651 (73708)	Allowed region, %	1.4
No. of unique reflections	56351 (15034)	Outlier region, %	0.0

[a]Values in parentheses refer to the highest resolution shell.

[b]$R_{sym} = \Sigma j \Sigma h |I_{h,j} - \langle Ih \rangle| / \Sigma j \Sigma h \, I_{h,j}$

[c]$R_{cryst} = \Sigma h |F_{obs} - F_{calc}| / \Sigma h \, F_{obs}$. R_{free} is calculated with a small fraction (5%) of reflections chosen to be part of a test group.

Table S3, related to Figure 3. Atomic charges calculated for the hydroxyphenyl moiety of the chromophore and interaction energies with its microenvironment.

(A) Comparison of the atomic charges in atomic units obtained with different methods (OPLS, PDDG/OPLS and PEOE) for the hydroxyphenyl moiety of the chromophore. (B) Statistics of the energies of interaction between the hydroxyphenyl moiety of the chromophore and its potential hydrogen-bonding partners in mEosFP and its variant M159A. The calculations are based on the last 200 ps of the atomistic simulations illustrated in Figure 3.

A	Atomic charges of phenolate			Atomic charges of phenol		
Atom	OPLS	PDDG/OPLS	PEOE	OPLS	PDDG/OPLS	PEOE
C_{para}	-0.21	-0.28	-0.03	-0.12	-0.15	-0.03
C_{meta}	-0.21	-0.04	-0.06	-0.12	-0.08	-0.06
H_{meta}	0.12	0.14	0.08	0.12	0.16	0.08
C_{ortho}	-0.21	-0.35	-0.05	-0.12	-0.26	-0.03
H_{ortho}	0.12	0.17	0.09	0.12	0.18	0.10
C	0.40	0.39	-0.01	0.15	0.13	0.04
O	-0.60	-0.53	-0.60	-0.58	-0.27	-0.60
H				0.43	0.27	0.41

B	Average Interaction Energy Phenol-Partner in kJ/mol (rmsd in brackets)			
Partner	mEosFP anionic	mEosFP neutral	mEosFP M159A anionic	mEosFP M159A neutral
Serine 142	-30.6 (9.4)	-19.7 (5.5)	-6.0 (2.6)	-23.5 (4.4)
Residue 159	-6.2 (7.6)	-14.4 (2.3)	-1.4 (0.3)	-0.4 (0.1)
W1 & W2	-46.2 (6.9)	-14.6 (4.3)	-92.7 (8.7)	-2.0 (1.4)

The OPLS charges were used for pKa calculations, atomistic simulations and calculation of interaction energies. Löwdin charges were obtained from hybrid PM3-PDDG/OPLS calculations, which provide reference values for the chromophore (QM region) within the mEosFP protein matrix (MM region). PEOE charges (Czodrowski et al., 2006) of the chromophore *in vacuo* were used for the initial optimization of the protein hydrogen bonds network with the PDB2PQR program (Dolinsky et al., 2007).

EXPERIMENTAL PROCEDURES

Photoconversion and photoswitching measurements

For measuring green-to-red photoconversion, green protein solutions were irradiated during ~25 min with a 405-nm laser light (CUBE, Coherent, Santa Clara, California, USA) at a measured power density of 72.5 mW/cm^2 on the sample. All measurements were carried out in a cuvette filled with 50 µl of the protein solution, at a concentration that corresponds to an OD of 0.3 at the maximum excitation peak. An area overlapping the 3 × 3 mm dimensions of the cuvette opening was irradiated, so that the whole of the solution was irradiated. Increasing irradiation periods (20 times 5 s, 20 times 15 s, 20 times 30 s and 5 times 120 s) were interleaved by the measurement of an absorption spectrum (3.8 ms acquisition time).

For reversible photoswitchings of green forms, the proteins were switched off by illuminating the samples with a 488-nm laser light (163 Series Argon-ion, Spectra-Physics, Irvine, California, USA) during 5 min at a measured power density of 37.5 mW/cm^2 on the sample. Back-switching to the on state was achieved by irradiating the sample with a 405-nm laser light (CUBE, Coherent) during 5 min at a measured power density of 2.2 mW/cm^2 on the sample.

For the red forms, the same protocol of reversible photoswitching was used but the on-off switching was either performed at 561 nm or 532 nm, depending on the absorption maximum of the protein. Proteins that were switched off with a 532-nm laser light (Excelsior 532-200-C1, Spectra-Physics), were illuminated at a measured power density of 40 mW/cm^2 while proteins that were switched off with a 561-nm laser light (Excelsior 561C-75, Spectra-Physics) were illuminated at a measured power density of 26.2 mW/cm^2. Proteins were backswitched to their bright state by irradiation at 440-nm laser light (Excelsior 440C-40, Spectra-Physics) at a measured power density of ~1.5 mW/cm^2 on the sample.

For both green and red on- and off-switching, constant irradiation periods of 6 s were interleaved with the acquisition of an absorption spectrum with the minimal lamp exposure (38 ms) leading to the 50 spectra during the off-switching and 50 spectra during the on-switching. Kinetics of both green or red

reversible photoswitchings and green-to-red photoconversions were fitted with a stretched exponential function,

$$y = A_1 \cdot \exp(-(\tau / t)^{\beta}) + A_0$$

Average phototransition times $<\tau>$ were determined according to the Gradshteyn and Rhyzhik integral

$$<\tau> = \frac{\tau}{\beta}\Gamma\left(\frac{1}{\beta}\right),$$

where Γ represents the gamma function and β the stretching parameter.

Analytical ultracentrifugation

Analytical ultracentrifugation measurements were performed as previously described (Mizuno et al., 2010). Briefly, we used the ProteomeLab XL-A ultracentrifuge (Beckman Coulter, Fullerton, California, USA) for the analytical equivalent centrifugation. The concentration of the sample was adjusted to an optical density of 0.5 in a 1-cm cuvette at the wavelength of maximum absorbance before centrifugation at 42×10^3 *g* for 22 h. The absorbance profile at the maximum excitation wavelength was monitored and fitted with a self-association model (McRorie and Voelker, 1993) in which the protein either associates as a dimer:

$$C_{total}(r) = C_m(r_0) \cdot e^{\frac{\omega^2}{2RT}M(1-\bar{\upsilon}\rho)(r^2-r_0^2)} + K'_{12}[C_m(r_0)]^2 \cdot e^{\frac{\omega^2}{2RT}2M(1-\bar{\upsilon}\rho)(r^2-r_0^2)}$$

or associates as a dimer and a tetramer:

$$C_{total}(r) = C_m(r_0) \cdot e^{\frac{\omega^2}{2RT}M(1-\bar{\upsilon}\rho)(r^2-r_0^2)} + K'_{12}[C_m(r_0)]^2 \cdot e^{\frac{\omega^2}{2RT}2M(1-\bar{\upsilon}\rho)(r^2-r_0^2)} + K'_{14}[C_m(r_0)]^4 \cdot e^{\frac{\omega^2}{2RT}4M(1-\bar{\upsilon}\rho)(r^2-r_0^2)}$$

K'_{12} and K'_{14} are the association coefficients for dimerization and tetramerization in weight concentration, respectively, $C_{total}(r)$ is the weight concentration of protein at position r, $C_m(r_0)$ is the concentration of monomeric protein at the meniscus, ω is the angular velocity, r_0 is the radius at the meniscus, R is the universal gas constant, T is the thermodynamic temperature, M is the molecular weight of protein, $\bar{\upsilon}$ is the partial specific volume and ρ is the density of solvent.

Molecular dynamics

The pKa of titrable residues was calculated with a recent release of the H++ web server (Gordon et al., 2005) that includes the REDUCE program (Word et al., 1999) to predict the most likely histidine tautomers (courtesy of Alexei Onufriev; http://biophysics.cs.vt.edu). We included either the anionic or the neutral chromophore in the models, by using atomic charges from the OPLS-AA force field (Jorgensen et al., 1996). Dielectric constants of 6 and 80 were used inside the protein and the solvent, respectively, for the calculation of electrostatic interactions. The Poisson-Boltzmann equation was used to calculate the desolvation penalty. The screening effects of the salt were included, considering a concentration of 0.15 M. All residues were determined to have their expected protonation in the range of pH under consideration. We can notice that Glu212 displayed negative pKa values and that His194 was unambiguously determined in its biprotonated form.

The protonated models were solvated in a water box with sodium ions to ensure charge neutrality of the overall system. The OPLS-AA force field was applied to the protein (Jorgensen et al., 1996), while the TIP3P model was used for the water molecules (Jorgensen et al., 1983). Since the chromophore is formed by three amino acids, we chose suitable parameters from the OPLS-AA force field. A good agreement exists between the OPLS charges and those issuing from other methods (see Table S1), which guarantees accurate results of the computational study. Periodic boundary conditions were applied, and nonbonding interactions were calculated by using an atom-based force-switching truncation function with inner and outer cut-offs of 8 Å and 12 Å, respectively (Field et al., 2000).

First, we optimized all atomic positions of the protein by using a conjugate gradient algorithm with an integration step of 10^{-3} Å, until the root mean square of the force components reaches 10^{-1} kJ.mol^{-1}.Å^{-1}. Then, we performed Langevin molecular dynamics (MD) simulations at 300 K with an integration step of 1 fs and a collision frequency of 25 ps^{-1}. Residues and water molecules having atoms less than 12 Å from the hydroxyl group of the chromophore were allowed to move, while the remaining part of the

system was fixed. The equilibration of the temperature and the potential energy were reached before performing 500 ps of MD simulations.

PALM analysis and image reconstruction

PALM images were acquired using an Olympus IX-71 inverted microscope, equipped with a PlanApochromat60×/1.4 objective lens (Olympus), a Z442/488/568RPC dichroic mirror (Chroma Technology Inc, Rockingham, Vermont, USA) and an EM-CCD camera (ImagEM, Hamamatsu Photonics, Hamamatsu City, Japan) with 512 × 512 pixels and an acquisition rate of 30 ms per frame. A 405-nm laser (Excelsior 405C-100, Spectra Physics) was used to photoconvert the fluorescent proteins. Green and red species were excited with a 488-nm laser (Excelsior-488, Spectra-Physics, ~125 W/cm^2) and a 561-nm laser (Excelsior 561C-75, Spectra-Physics, ~110 W/cm^2) illumination in Köhler mode, respectively. Green-to-red photoconversion was achieved by irradiating the sample with the 405-nm laser (~7 W/cm^2 on the sample) for 20-30 s. The fluorescence image was acquired through an HQ527/30M band pass filter (Chroma Technology Inc.) for the green state and HQ595/40M band pass filter (Chroma Technology Inc.) for the red state. The image was further magnified 3.3 × with a tube lens, resulting in a maximum field of view of 41 × 41 μm^2 (80 × 80 nm^2 per pixel) on the EM-CCD chip.

The acquired data were analyzed using a home-made software package, the details of which will be reported elsewhere. Briefly, prospective emitters in each frame were localized using nonlinear least squares fitting of a two-dimensional symmetric Gaussian function. The quality of each fit was verified by comparing the fitted amplitude with the local background, and by requiring that the fitted standard deviation was within 50% of the theoretically expected value, with unsuccessful localizations being discarded. Additionally localizations that were judged to be too close to one another for interference-free localization (within 4 times the standard deviation of the PSF) were discarded. The resulting dataset was then analyzed to recognize those situations where single emitters were active over multiple frames, combining these into a single event. This postprocessing step prevents these emitters from appearing

with undue weight compared to those that are only present in a single frame, and also allows an estimate of the localization error by comparing subsequent localizations of the same emitter, which is the value reported in the main text.

REFERENCES

Adam, V., Lelimousin, M., Boehme, S., Desfonds, G., Nienhaus, K., Field, M.J., Wiedenmann, J., McSweeney, S., Nienhaus, G.U., and Bourgeois, D. (2008). Structural characterization of IrisFP, an optical highlighter undergoing multiple photo-induced transformations. Proc Natl Acad Sci U S A 105, 18343-18348.

Ando, R., Flors, C., Mizuno, H., Hofkens, J., and Miyawaki, A. (2007). Highlighted generation of fluorescence signals using simultaneous two-color irradiation on Dronpa mutants. Biophys J 92, L97-99.

Ando, R., Mizuno, H., and Miyawaki, A. (2004). Regulated fast nucleocytoplasmic shuttling observed by reversible protein highlighting. Science 306, 1370-1373.

Andresen, M., Stiel, A.C., Folling, J., Wenzel, D., Schonle, A., Egner, A., Eggeling, C., Hell, S.W., and Jakobs, S. (2008). Photoswitchable fluorescent proteins enable monochromatic multilabel imaging and dual color fluorescence nanoscopy. Nat Biotechnol 26, 1035-1040.

Czodrowski, P., Dramburg, I., Sotriffer, C.A., and Klebe, G. (2006). Development, validation, and application of adapted PEOE charges to estimate pK(a) values of functional groups in protein-ligand complexes. Proteins 65, 424-437.

Dolinsky, T.J., Czodrowski, P., Li, H., Nielsen, J.E., Jensen, J.H., Klebe, G., and Baker, N.A. (2007). PDB2PQR: expanding and upgrading automated preparation of biomolecular structures for molecular simulations. Nucleic Acids Res 35, W522-W525.

Field, M.J., Albe, M., Bret, C., Proust-De Martin, F., and Thomas, A. (2000). The Dynamo library for molecular simulations using hybrid quantum mechanical and molecular mechanical potentials. J Comput Chem 21, 1088-1100.

Fuchs, J., Bohme, S., Oswald, F., Hedde, P.N., Krause, M., Wiedenmann, J., and Nienhaus, G.U. (2010). A photoactivatable marker protein for pulse-chase imaging with superresolution. Nat Methods.

Gordon, J.C., Myers, J.B., Folta, T., Shoja, V., Heath, L.S., and Onufriev, A. (2005). H++: a server for estimating pK(a)s and adding missing hydrogens to macromolecules. Nucleic Acids Res 33, W368-W371.

Gurskaya, N.G., Verkhusha, V.V., Shcheglov, A.S., Staroverov, D.B., Chepurnykh, T.V., Fradkov, A.F., Lukyanov, S., and Lukyanov, K.A. (2006). Engineering of a monomeric green-to-red photoactivatable fluorescent protein induced by blue light. Nat Biotechnol 24, 461-465.

Jorgensen, W.L., Chandrasekhar, J., Madura, J.D., Impey, R.W., and Klein, M.L. (1983). Comparison of Simple Potential Functions for Simulating Liquid Water. J Chem Phys 79, 926-935.

Jorgensen, W.L., Maxwell, D.S., and TiradoRives, J. (1996). Development and testing of the OPLS all-atom force field on conformational energetics and properties of organic liquids. J Am Chem Soc 118, 11225-11236.

McRorie, D.K., and Voelker, P.J. (1993). Self-associating systems in the analytical ultracentrifuge (Palo Alto, California: Beckman Instruments, Inc.).

Mizuno, H., Dedecker, P., Ando, R., Fukano, T., Hofkens, J., and Miyawaki, A. (2010). Higher resolution in localization microscopy by slower switching of a photochromic protein. Photochem Photobiol Sci 9, 239-248.

Stiel, A.C., Trowitzsch, S., Weber, G., Andresen, M., Eggeling, C., Hell, S.W., Jakobs, S., and Wahl, M.C. (2007). 1.8 A bright-state structure of the reversibly switchable fluorescent protein Dronpa guides the generation of fast switching variants. Biochem J 402, 35-42.

Wiedenmann, J., Ivanchenko, S., Oswald, F., Schmitt, F., Rocker, C., Salih, A., Spindler, K.D., and Nienhaus, G.U. (2004). EosFP, a fluorescent marker protein with UV-inducible green-to-red fluorescence conversion. Proc Natl Acad Sci U S A 101, 15905-15910.
Word, J.M., Lovell, S.C., Richardson, J.S., and Richardson, D.C. (1999). Asparagine and glutamine: Using hydrogen atom contacts in the choice of side-chain amide orientation. J Mol Biol 285, 1735-1747.